Commun Nonlinear Sci Numer Simulat 156 (2026) 109646

Contents lists available at ScienceDirect

Communications in Nonlinear Science and Numerical Simulation

journal homepage: www.elsevier.com/locate/cnsns

Research paper

A numerical analysis of planar colliding binary companions

G. A. Caritá[a,b,*], V. M. de Oliveira[c,d], S. Mottola[b], D. L. Silva[e], S. Aljbaae[a,f], H. Hussmann[b], K. Willner[b], A. F. B. A. Prado[a]

[a] PPG em Engenharia e Tecnologia Espacial, INPE, São José dos Campos, 12227-010, Brazil
[b] Institute of Space Research, DLR, Berlin, 12489, Germany
[c] Instituto de Matemática, Estatística e Ciência da Computação, Universidade de São Paulo, São Paulo, 05508-090, Brazil
[d] CFisUC, Departamento de Física, Universidade de Coimbra, Coimbra, 3004-516, Portugal
[e] Departamento de Ciências da Natureza, Matemática e Educação, Universidade Federal de São Carlos, Araras, 13600-970, Brazil
[f] Instituto de Astronomía y Ciencias Planetarias, Universidad de Atacama, Copiapó, 485, Chile

ARTICLE INFO

Keywords:
Asteroids
Collision
Binaries
Celestial mechanics

ABSTRACT

In the last few years, many interesting objects were discovered in the Solar System, such as the asteroid Arrokoth, a contact binary which was observed by NASA's New Horizons mission. Understanding the dynamics of this type of objects is essential for unraveling the history of the Solar System, as collisions during the early stages of their formation may have significantly influenced their evolution. In this study, we propose that low-speed, non-elastic collisions could play a critical role in the formation of contact binaries. To investigate this, we model the dynamics of colliding binary systems using a numerical approach based on the full two-body problem (F2BP) in a planar configuration assuming rigid bodies. The equations of motion are solved numerically, with collisions handled by an ellipsoid overlap detection algorithm along with an impulse response model. Non-elastic collisions are considered by incorporating energy dissipation through a velocity-dependent model based on the relative velocity between the bodies and a constant coefficient of restitution (COR). The simulations yield three possible outcomes: merge, bound, and escape configurations. From random sampling simulation on the full phase space for different bodies' shapes, we observed an nearly constant percentage of escape cases ($\sim 60\%$) going from an almost perfectly elastic (COR = 0.9) to an almost perfectly inelastic (COR = 0.1) collision scenario. The other cases have shown a dependent relation as we varied the coefficient of restitution, with the percentage of merge cases decreasing from $\sim 34.6\%$ to $\sim 26\%$ and the percentage of bounded cases increasing from $\sim 8.4\%$ up to $\sim 20.2\%$. We apply our methodology to Antiope and Arrokoth, and we find that these systems present a higher likelihood of staying at their current state, namely, bounded for the former and merged for the latter. These results highlight that collisions are a significant energy dissipation mechanism and could play an important role in the formation of binary systems.

1. Introduction

Collisional dynamics is a very relevant topic in celestial mechanics since collisions between celestial bodies play an important role in shaping their evolution, composition, and eventual fate. However, modeling the intricate dynamics of these collisions poses substantial challenges due to the complex interplay of gravitational forces, rotational motion, and dissipative processes.

* Corresponding author.
E-mail address: gabriel.carita@inpe.br (G.A. Caritá).

https://doi.org/10.1016/j.cnsns.2026.109646
Received 29 September 2025; Received in revised form 18 December 2025; Accepted 5 January 2026
Available online 8 January 2026

Numerous studies have explored the dynamics of collisions within the celestial realm, each providing unique insights into the phenomena at play. Ćuk [1] presented a significant reassessment of our understanding of binary asteroids, focusing particularly on the origins and evolution of small binary near-Earth asteroids (NEAs). By incorporating Yarkovsky effects (YORP), they proposed a novel explanation for the formation of kilometer-sized binary NEAs, challenging earlier assumptions about their origins through planetary encounters. According to Taylor and Margot [2], asteroids that remain bound after an impact could evolve into unstable orbits or fully synchronous orbits depending on the amount of angular momentum injected by YORP or Binary-YORP.

Bottke and Melosh [3] developed a comprehensive model to explain the formation of double-impact craters on Earth, Venus, and Mars. Their study suggested that fast-rotating rubble-pile asteroids undergoing close planetary encounters may experience a tidal breakup, resulting in stable binary systems that subsequently impact planets, thus creating distinct twin craters. Furthermore, as discussed in Pravec et al. [4], photometric observations support the hypothesis that asteroid pairs form through rotational fission. Scheeres [5] examined the stability and outcomes of strongly interacting binary asteroid systems, elucidating the transfer of energy and angular momentum between rotational and translational motion under the assumption of energy dissipation. Several others studies have investigated the dynamics of a system composed of two solid bodies, such as Scheeres [6], Fahnestock and Scheeres [7], Hou et al. [8], Tricarico [9], Conway [10], Lu et al. [11], Ho [12].

Particularly in contexts such as Saturn's rings and asteroid formation, collisions have been studied extensively [13–17]. In collision dynamics, energy dissipation is often related to a critical velocity below which collisions are perfectly elastic [16,18,19]. According to Dilley [15] and Dilley and Crawford [16], for frosted small ice spheres the collision forces become speed-dependent. Durda et al. [20] experiments with meters-sized granite spheres yield uncertain results. The derived coefficient of restitution (COR) was 0.83 for speeds up to approximately $1m/s$. However, for lower speeds, the curves displayed large error bars, and the experimentally measured values of the COR tend to unity, indicating elastic collisions. The dynamical response of the material remains uncertain, particularly since no experiments have been conducted with larger sizes and masses. In this study, we adopt the COR as a free constant parameter ranging from an almost perfectly elastic (COR = 0.9) to an almost perfectly inelastic (COR = 0.1) case.

An interesting example where collisions might be important is Antiope, a close binary asteroid system where both bodies have approximately the same mass and size, and their size to distance ratio is about $1/4$ [21]. Another noteworthy object is (486958) Arrokoth, initially believed to have been formed from two separate bodies that gradually spiraled inward until contact, with collisions and friction between particles contributing to the process [22]. However, uncertainties remain regarding the role of collisions in the formation of such objects and how significant these events are in their development.

In this study, we are interested in understanding the role of low-velocity collisions in the formation of contact binaries. To address this question we employ a comprehensive numerical model, based on the full two-body problem (F2BP) in a planar configuration, that simulates the motion of ellipsoidal bodies taking into account their rotational dynamics. We also implement an algorithm to detect collisions between the objects which are solved via an impulse-response model. Energy dissipation is investigated through collisions for various object sizes, densities, masses and restitution coefficients, allowing us to explore the diverse behaviors of colliding binary systems. We assume perfectly frictionless collisions and rigid non-deformable bodies.

This manuscript is organized as follows. Section 2 introduces the dynamical model. Sections 3 and 4 describe the numerical setup, collision detection and collision handling. Elastic collision and dissipation modeling are addressed in Section 5, and random sampling simulations are performed in Section 6. Our conclusions are then presented in Section 7.

2. Dynamical model

The mutual potential U_M for a binary system consisting of ellipsoidal bodies in the planar configuration, written as a 2nd order expansion in the moments of inertia, is given by [23]

$$U_M = -\frac{GM_1M_2}{R}\left\{1 + \frac{1}{2R^2}\left[\mathrm{Tr}\,\bar{\boldsymbol{I}}_1 + \mathrm{Tr}\,\bar{\boldsymbol{I}}_2 - \frac{3}{2}\left(\bar{I}_{1x} + \bar{I}_{2x} + \bar{I}_{1y} + \bar{I}_{2y} - (\bar{I}_{1y} - \bar{I}_{1x})\cos 2\phi_1 - (\bar{I}_{2y} - \bar{I}_{2x})\cos 2\phi_2\right)\right]\right\}, \tag{1}$$

where G is the gravitational constant, R is the separation of the binary system measured with respect to the center of mass of each body, M_1 and M_2 are the masses of the primary and the secondary, respectively, and $\bar{\boldsymbol{I}}_i = \boldsymbol{I}_i\ /M_i$ is the mass-normalized inertia tensor of each body $i = 1, 2$, with principal moments of inertia denoted by $\bar{I}_{ix}, \bar{I}_{iy}, \bar{I}_{iz}$. The operator Tr is the usual trace function, and ϕ_1 and ϕ_2 represent the orientation of each body with respect to the body-connecting line. A schematic of the system is presented in Fig. 1. Here, we take both the gravitational constant and the total mass of the system as unity. In this case, $M_2 = \mu$ corresponds to the secondary body, while $M_1 = 1 - \mu$ corresponds to the primary body, where $\mu = M_2/(M_1 + M_2)$ is the system's mass ratio. We consider the planar case, where both bodies rotate perpendicularly to the orbital plane.

The equations of motion can be derived directly from the Lagrangian of the system, as detailed in Scheeres [23], and are given by

$$\ddot{R} = \dot{\theta}^2 R - \frac{1}{m}U_{M,R}, \tag{2a}$$

$$\ddot{\phi}_1 = -\left(1 + \frac{mR^2}{I_{1z}}\right)\frac{1}{mR^2}U_{M,\phi_1} - \frac{1}{mR^2}U_{M,\phi_2} + \frac{2}{R}\dot{R}\,\dot{\theta}, \tag{2b}$$

$$\ddot{\phi}_2 = -\left(1 + \frac{mR^2}{I_{2z}}\right)\frac{1}{mR^2}U_{M,\phi_2} - \frac{1}{mR^2}U_{M,\phi_1} + \frac{2}{R}\dot{R}\,\dot{\theta}, \tag{2c}$$

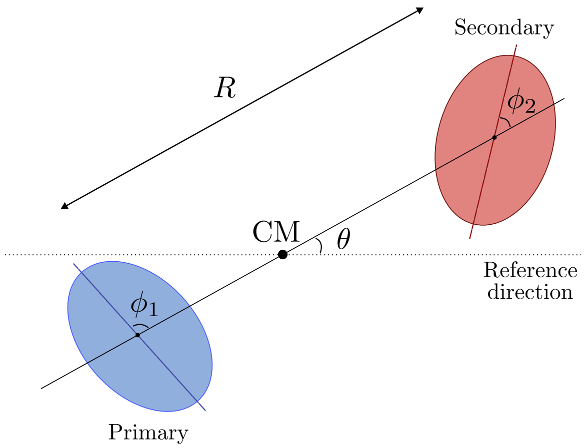

Fig. 1. Description of the planar full two-body problem, where the distance between the bodies is R, the rotation angle of the line connecting the bodies is θ, and the rotation angle of the bodies relative to this line is ϕ_1 (primary) and ϕ_2 (secondary). CM stands for center of mass, θ is measured with respect to a reference direction, which is marked with a dotted line, and ϕ_1 and ϕ_2 are measured with respect to the longest physical axis of each body, which are marked with dashed lines.

$$\ddot{\theta} = \frac{1}{mR^2}U_{M,\phi_1} + \frac{1}{mR^2}U_{M,\phi_2} - \frac{2}{R}\dot{R}\,\dot{\theta}, \tag{2d}$$

with $U_{M,R}$, U_{M,ϕ_1}, and U_{M,ϕ_2} being the partial derivatives of the mutual potential U_M with respect to R, ϕ_1, and ϕ_2, respectively. The term $m = M_1M_2/(M_1+M_2)$ is the reduced mass of the system, while $\dot{\phi}_1$ and $\dot{\phi}_2$ are the angular velocities of the primary and the secondary in the z-axis. As shown in Fig. 1, θ and $\dot{\theta}$ describe the orientation and the angular velocity of the binary relative to a predefined inertial direction.

In our investigation, we consider each body as a tri-axial ellipsoid with physical axes $a \geq b \geq c$ parametrized as

$$a = a_0, \tag{3a}$$
$$b = a_0(1-f) + c_0 f, \tag{3b}$$
$$c = b_0(1-f) + c_0 f, \tag{3c}$$

where a_0, b_0, and c_0 are arbitrary parameters and f is the geometric eccentricity of the body. By changing these parameters, we can impose different body shapes ranging from an oblate spheroid, with $f = 0$ and $a_0 \neq b_0$, to a prolate spheroid, with $f = 1$ and $a_0 \neq c_0$. If we set $a_0 = b_0 = c_0$, the body shape is reduced to a perfect sphere.[1]

Finally, assuming a constant mass density throughout the entire ellipsoidal body, the principal mass-normalized moments of inertia can then be calculated via

$$\bar{I}_x = \frac{1}{5}\left(b^2 + c^2\right), \tag{4a}$$
$$\bar{I}_y = \frac{1}{5}\left(a^2 + c^2\right), \tag{4b}$$
$$\bar{I}_z = \frac{1}{5}\left(a^2 + b^2\right). \tag{4c}$$

3. Numerical setup and collision detection

We implemented a detailed numerical setup to accurately solve and track the system dynamics. The differential equations were solved numerically using the JULIA programming language with the VERN9 method. The absolute error tolerance was set to 10^{-12}, ensuring high precision, with elastic cases conserving energy to approximately a level of 10^{-13}. To detect collisions between the ellipsoids, we monitored each simulation step using the ContinuousCallback feature of the *DifferentialEquations* package, which locates the exact moment of a collision event via a root-finding method [24].

In order to detect collisions between these ellipsoids it is enough to detect collisions between the ellipses that describe the bodies equators. Such collisions were verified using a robust method, which involves expressing ellipses in matrix form. The center-oriented

[1] The flattening and elongation of each ellipsoidal body can be defined as $1 - c/a$ and $1 - b/a$, respectively. The axis ratios a/c and a/b are used in our analysis in Section 6.

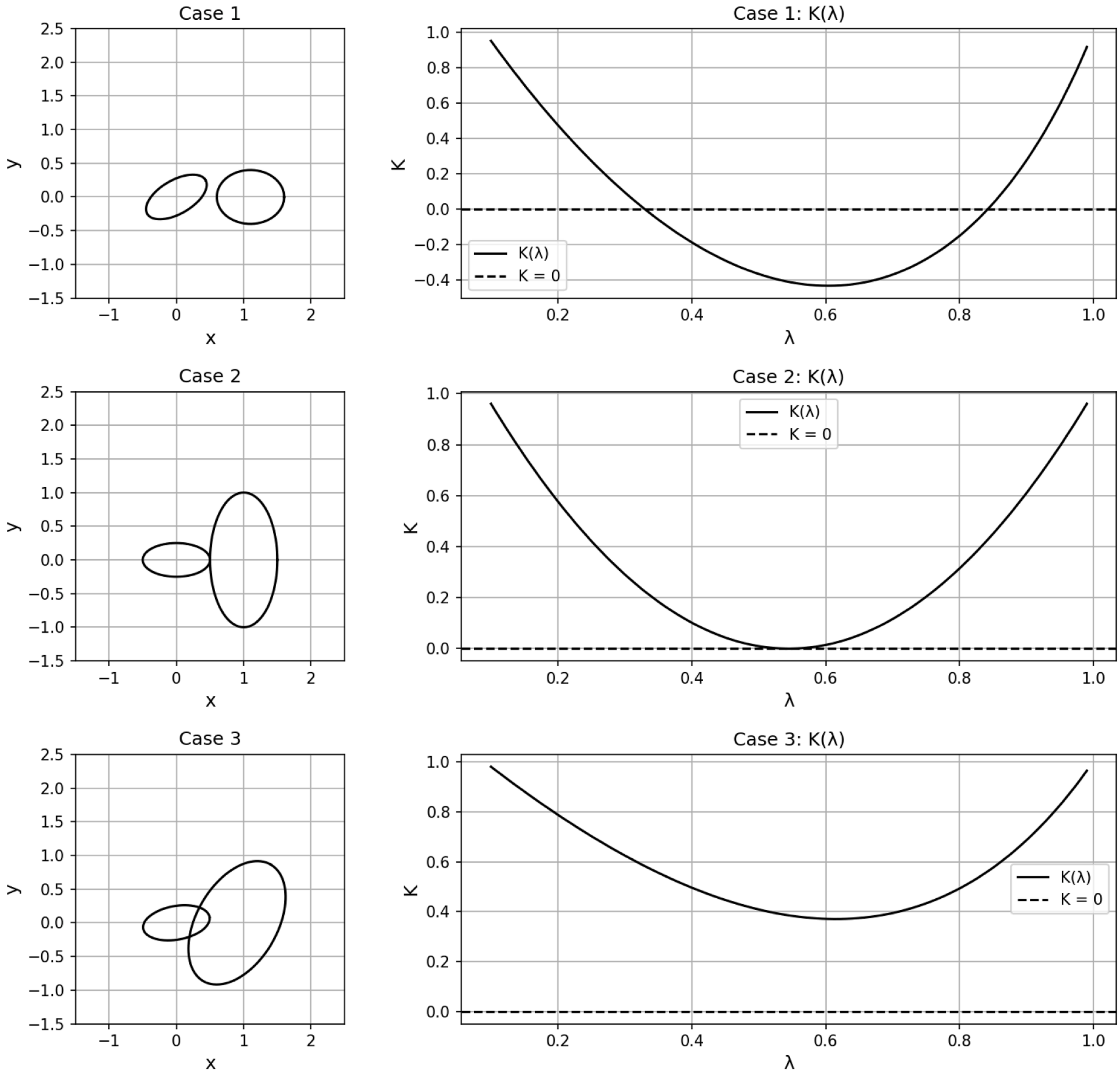

Fig. 2. Detection method for collisions between two ellipsoids in the planar case. Left panels show different possible scenarios, while right panels plot $K(\lambda)$ as a function of λ for each situation. Horizontal lines in the right panels highlight $K = 0$ for reference.

form of a standard ellipse can be described as [25]

$$1 = \frac{x^2}{a^2} + \frac{y^2}{b^2} = \begin{bmatrix} x & y \end{bmatrix} \begin{bmatrix} \frac{1}{a^2} & 0 \\ 0 & \frac{1}{b^2} \end{bmatrix} \begin{bmatrix} x \\ y \end{bmatrix} =: \mathbf{X}^T D \mathbf{X}, \tag{5}$$

where the superscript T denotes the transpose operation. Additionally, in order to account for the ellipse orientation, its matrix form may be rotated using a rotation matrix $\mathcal{R}(\alpha)$, defined as

$$\mathcal{R} = \begin{bmatrix} \cos\alpha & -\sin\alpha \\ \sin\alpha & \cos\alpha \end{bmatrix},$$

upon performing the following transformation $D \to \mathcal{R}^T D \mathcal{R}$.

Following Gilitschenski and Hanebeck [25], an overlap condition between two ellipsoids can be derived with the aid of a function $K(\lambda)$ given by

$$K(\lambda) = 1 - \mathbf{u}^T \left(\frac{1}{1-\lambda} \mathbf{B}^{-1} + \frac{1}{\lambda} \mathbf{A}^{-1} \right) \mathbf{u}, \tag{6}$$

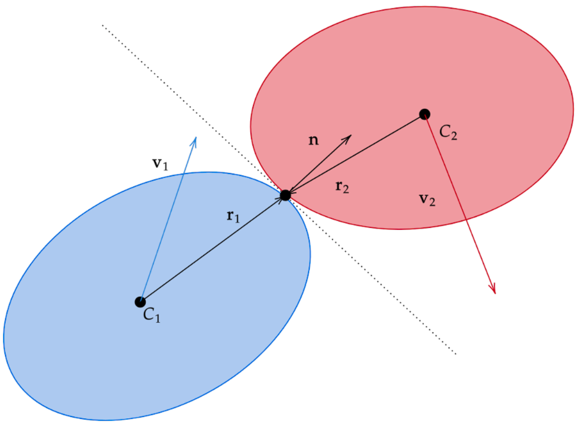

Fig. 3. Body-body collision model.

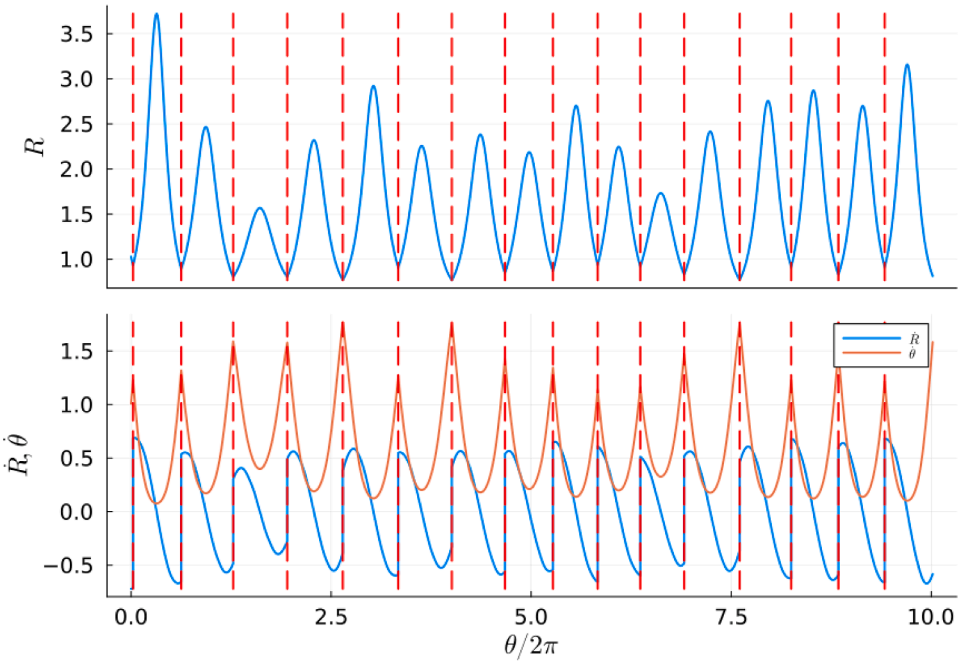

Fig. 4. Time evolution of some dynamical variables assuming an elastic condition (COR = 1). The initial conditions used for this figure are detailed in Appendix A. The red vertical lines indicate collision events. Semi-axes: $a_1 = 0.5$, $b_1 = 0.39787$, $c_1 = 0.32446$, $a_2 = 0.45$, $b_2 = 0.36533$, $c_2 = 0.32177$.

where the superscript -1 denotes an inverse matrix. Matrices $\mathbf{A}$ and $\mathbf{B}$ are the rotated matrix forms of the two ellipses,[2] $\mathbf{u}$ is the relative position vector between their centers, and λ is a parameter between zero and one. The relationship between the ellipsoids is then given by the minimum value of $K(\lambda)$ in the following manner:

- If $\min\limits_{\lambda} K(\lambda) > 0$, the ellipsoids are overlapping;
- If $\min\limits_{\lambda} K(\lambda) = 0$, the edges of the ellipsoids are in contact;
- If $\min\limits_{\lambda} K(\lambda) < 0$, the ellipsoids are not overlapping.

At each time step during the numerical integration, this equation is solved, and the minimum value of $K(\lambda)$ is determined using the Nelder-Mead optimization method [26]. If $\min K(\lambda) > 0$, the solver locates the collision moment with a threshold of $\delta = 10^{-12}$. Upon detecting a collision, an instantaneous impulse is applied following the model described in the next section, and the solver resumes the integration until the next collision event.

[2] The rotated matrix forms are obtained by following the transformation $A \to \mathcal{R}^T A \mathcal{R}$ and $B \to \mathcal{R}^T B \mathcal{R}$.

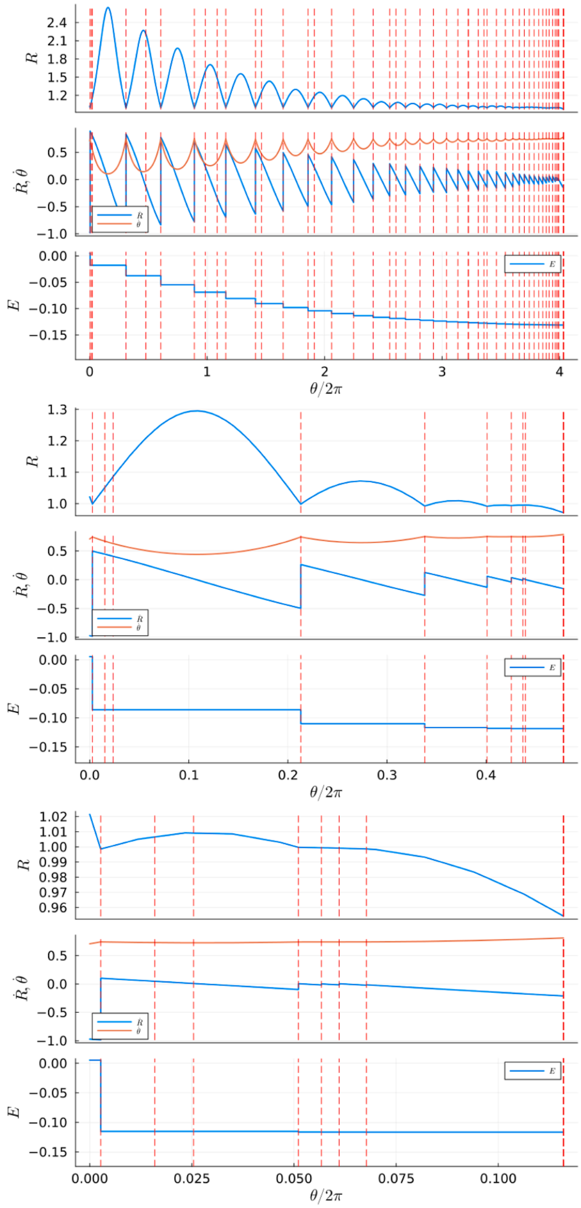

Fig. 5. Time evolution of some dynamical variables for ≈ 1.2 revolutions considering dissipation for COR $= 0.9$, 0.5 and 0.1 from top panel to bottom panel. The initial conditions used for this figure are detailed in Appendix A. The red vertical lines indicate collision events. Semi-axes: $a_1 = 0.5$, $b_1 = 0.49086$, $c_1 = 0.44086$, $a_2 = 0.5$, $b_2 = 0.5$, $c_2 = 0.45$.

Fig. 2 illustrates various scenarios and their corresponding $K(\lambda)$ values as a function of λ. The upper panels show a case where $\min K(\lambda) < 0$, indicating no overlap. The middle panels depict a scenario where the ellipsoids are in contact, with $\min K(\lambda) = 0$. Finally, the bottom panels show overlapping ellipsoids, where $\min K(\lambda) > 0$. In practice, we consider that a collision occurs when $0 < \min K(\lambda) < \delta$.

Simulations are terminated under two conditions: when escape occurs ($R > 30$) or when the binary system merges. Additionally, while the implementation of an instantaneous impulse at the moment of collision theoretically prevents penetration, numerical limitations such as high collision frequencies within small time intervals can sometimes lead to overlap due to unresolved collisions between consecutive steps. To address this issue, we enforce a maximum of 25,000 iterations to resolve collisions. If this limit is exceeded the simulation is also stopped.

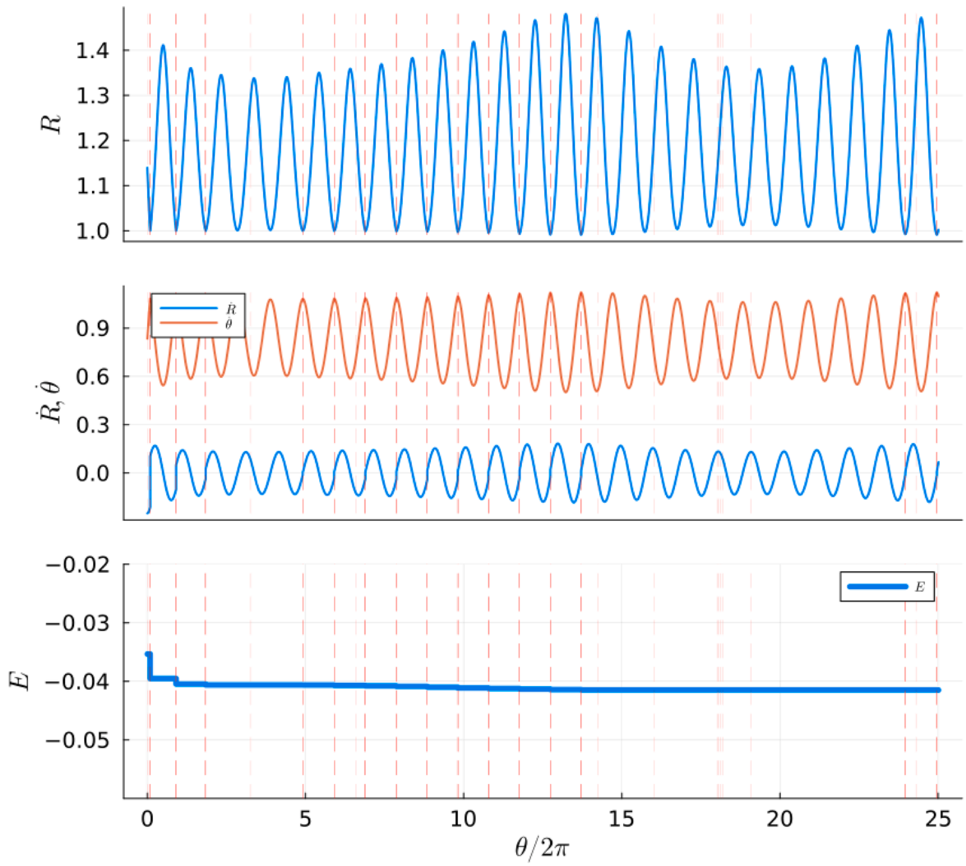

Fig. 6. Time evolution of some dynamical variables of a given bounded solution for 25 revolutions assuming COR = 0.5. The initial conditions used for this figure are detailed in Appendix A. The red vertical lines indicate collision events. Semi-axes: $a_1 = 0.5$, $b_1 = 0.49091$, $c_1 = 0.44091$, $a_2 = 0.5$, $b_2 = 0.49995$, $c_2 = 0.4499$.

4. Collision response

In this section, we describe our collision response method for interactions between two rigid bodies. We assume perfectly frictionless collisions, as detailed in Barraff [27].

Let $\mathbf{r}_1$ and $\mathbf{r}_2$ be the distances from the center of mass of the objects to the contact point, $\mathbf{v}_1$ and $\mathbf{v}_2$ the velocities of the ellipsoids' centers of mass, and $\dot{\phi}_1$ and $\dot{\phi}_2$ the angular velocities, as described in Fig. 3. Furthermore, let $\mathbf{\Omega}_1$ and $\mathbf{\Omega}_2$ be the angular velocity vector of each body. Since we are considering the planar case, we have that $\mathbf{\Omega}_1 = \dot{\phi}_1\hat{\mathbf{z}}$ and $\mathbf{\Omega}_2 = \dot{\phi}_2\hat{\mathbf{z}}$. With these definitions, the relative velocity $\mathbf{v}_{rel}$ at the point of contact can be written as

$$\mathbf{v}_{rel} = (\mathbf{v}_2 + \mathbf{\Omega}_2 \times \mathbf{r}_2) - (\mathbf{v}_1 + \mathbf{\Omega}_1 \times \mathbf{r}_1). \tag{7}$$

Now let $\mathbf{v}'_{rel}$ be the relative velocity at the contact point right after a collision. The Coefficient of Restitution (COR) models the change between the relative velocity before and after the collision along the direction normal to the collision plane, represented by the unitary vector $\mathbf{n}$, in the following manner

$$\mathbf{v}'_{rel} \cdot \mathbf{n} = -\mathrm{COR}\, \mathbf{v}_{rel} \cdot \mathbf{n}, \tag{8}$$

where the minus sign indicates that the relative velocity changes direction after the collision. The Coefficient of Restitution is then a dimensionless parameter that quantifies the elasticity of a collision between two bodies. COR equals 1 indicates a perfectly elastic collision where the objects rebound without any loss of rotational or kinetic energy energy. COR equals 0 represents a perfectly inelastic collision where the objects stick together after the impact, maximizing energy dissipation.

The collision response is modeled via an impulse $\mathbf{J}$ along the contact point. The change in the linear and the angular velocities are then given by

$$\Delta\mathbf{v}_1 = -\frac{1}{m_1}\mathbf{J}, \tag{9a}$$

$$\Delta\mathbf{v}_2 = \frac{1}{m_2}\mathbf{J}, \tag{9b}$$

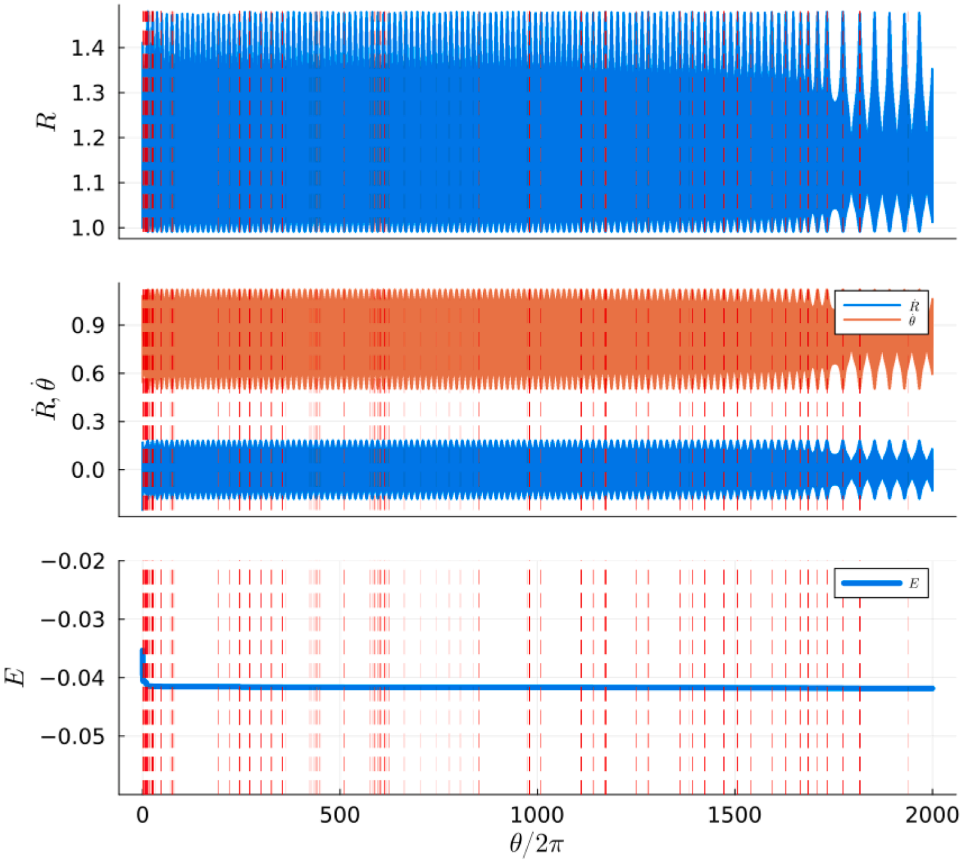

Fig. 7. Time evolution of some dynamical variables of a given bounded solution for 2000 revolutions assuming COR = 0.5. The initial conditions used for this figure are detailed in Appendix A. The red vertical lines indicate collision events. Semi-axes: $a_1 = 0.5$, $b_1 = 0.49091$, $c_1 = 0.44091$, $a_2 = 0.5$, $b_2 = 0.49995$, $c_2 = 0.4499$.

$$\Delta\mathbf{\Omega}_1 = -\mathbf{I}_1^{-1}(\mathbf{r}_1 \times \mathbf{J}), \tag{9c}$$

$$\Delta\mathbf{\Omega}_2 = \mathbf{I}_2^{-1}(\mathbf{r}_2 \times \mathbf{J}). \tag{9d}$$

Substituting into Eq. (8) the expression for the relative velocities before and after the collision, Eq. (7), and using the differences between the linear and angular velocities due to the collision, Eq. (9), we arrive at an expression for the magnitude J of the impulse as a function of the Coefficient of Restitution given by

$$J = \frac{-(1 + \mathrm{COR})\, \mathbf{v}_{rel} \cdot \mathbf{n}}{m_1^{-1} + m_2^{-1} + [\, \mathbf{I}_1^{-1}\, (\mathbf{r}_1 \times \mathbf{n}) \times \mathbf{r}_1 + \mathbf{I}_2^{-1}\, (\mathbf{r}_2 \times \mathbf{n}) \times \mathbf{r}_2\,] \cdot \mathbf{n}}. \tag{10}$$

Finally, the post-collision values for the radial separation velocity and the binary orbital velocity are given by

$$|\dot{R}|' = ||\mathbf{v}_2' - \mathbf{v}_1'||, \tag{11a}$$

$$\dot{\theta}' = \frac{x_1 \mathbf{v}_{rel,y}' - y_1 \mathbf{v}_{rel,x}'}{x_1^2 + y_1^2}, \tag{11b}$$

where x_1 and y_1 are the Cartesian coordinates of the primary ellipsoid's center of mass, and $\mathbf{v}_{rel,x}'$ and $\mathbf{v}_{rel,y}'$ are the components in the $x-$ and $y-$ directions of the post-collision relative velocity, respectively.

In our simulations, we assume a constant COR and we use Eq. (10) to determine the impulse for a given dynamical setting, later using this value to update the system velocities via Eqs. (9) and (11).

5. Perfectly elastic collisions and energy dissipation

In the case of perfectly elastic collisions, no energy dissipation occurs, which is often a reasonable assumption for low-velocity collisions [16,18,19]. Dilley and Crawford [16] showed that as the radii of small viscous icy spheres increase, these objects tend

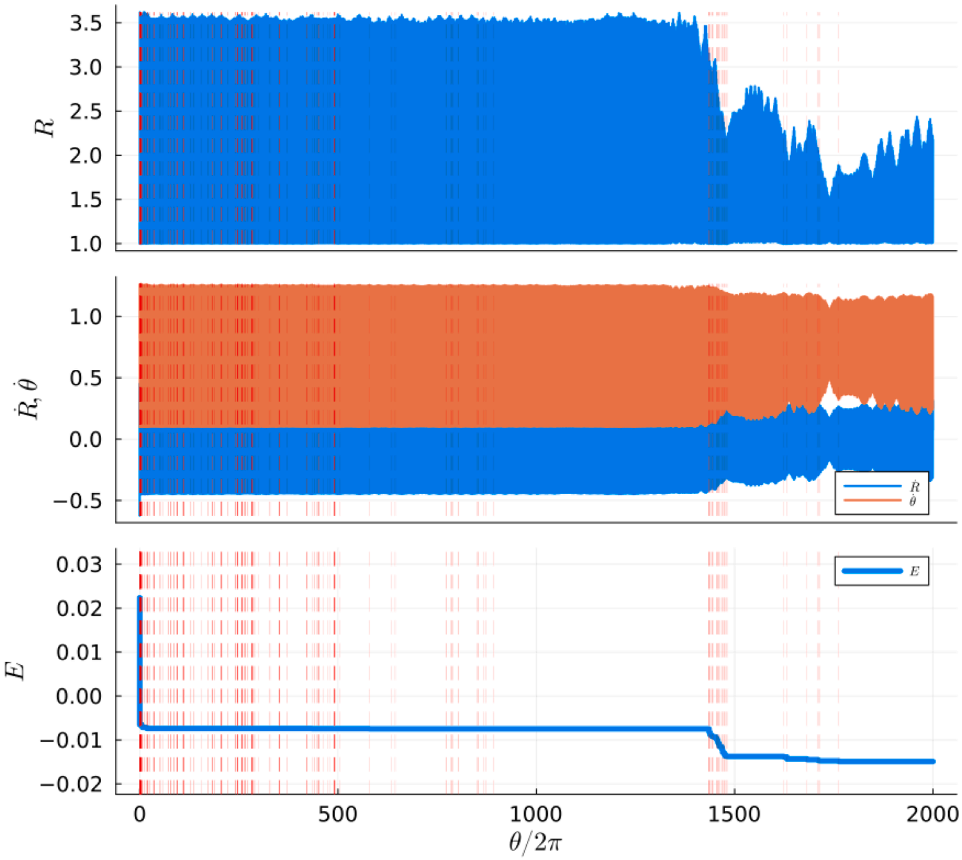

Fig. 8. Time evolution of some dynamical variables of a given bounded solution for 2000 revolutions assuming COR = 0.1. In this example, the collisions stop after 1300 revolutions. The initial conditions used for this figure are detailed in Appendix A. The red vertical lines indicate collision events. Semi-axes: $a_1 = 0.5$, $b_1 = 0.495454$, $c_1 = 0.445454$, $a_2 = 0.5$, $b_2 = 0.495454$, $c_2 = 0.445454$.

to retain a significant portion of its initial velocity when rebounding with other objects. In the dynamics of icy particles, however, energy loss plays a significant role during collisions. For example, in the dynamics of ring formation such as in Saturn, the coefficient of restitution (COR) is an important parameter [14].

For asteroid dynamics, there are a few ways to dissipate energy: by removing particles or dust during contact, by ejecting particles from the system, or by transforming kinetic energy into heat during collisions. For low-speed collisions, the heat generated is small enough to be neglected, and lifted particles would have a sufficiently small escape velocity to be neglected. However, as shown in Durda et al. [20], the impact of larger bodies is likely to dissipate significant energy. As discussed in Dilley and Crawford [16], for centimeter-sized objects, with increasing mass, the dependence on velocity becomes less significant for overall dynamics, although its exact impact on larger bodies remains uncertain. That being said, when energy dissipates in our adopted two-body model, given by Scheeres [23], the angular momentum must be conserved.

It is important to stress that extrapolating models from small-scale collisions to collisions between asteroids is hard, especially because said experiments are mainly done in laboratory settings with certain type of materials such as ice, while asteroids have different compositions, including other factors such as surface roughness, porosity, rubble-pile structures. To address this issue without losing generality, we analyze the system for different (constant) values of the COR, therefore reproducing different scenarios of energy dissipation.

The variable $\dot{R} = V_R$ represents the relative speed between the centers of mass of both bodies. At the moment of collision, we use COR as a factor to update the new $\dot{R}$ using the equations described in Section 4. To assess dissipation and energy deviation (ΔE), we use the reduced energy of the system (E) given by Eq. (12), which is an integral of motion for the planar case defined by Scheeres [23]. The total angular momentum is given by Eq. (13). It is worth noting that the constants (E and L) are maintained in elastic collisions.

$$E = \frac{1}{2}\frac{L^2 - \left(I_{1z}\dot{\phi}_1 + I_{2z}\dot{\phi}_2\right)^2}{I_z} + \frac{1}{2}\left(I_{1z}\dot{\phi}_1^2 + I_{2z}\dot{\phi}_2^2 + m\dot{r}^2\right) + V \tag{12}$$

$$L = \left(I_{1z} + I_{2z} + mr^2\right)\dot{\theta} + I_{1z}\dot{\phi}_1 + I_{2z}\dot{\phi}_2 \tag{13}$$

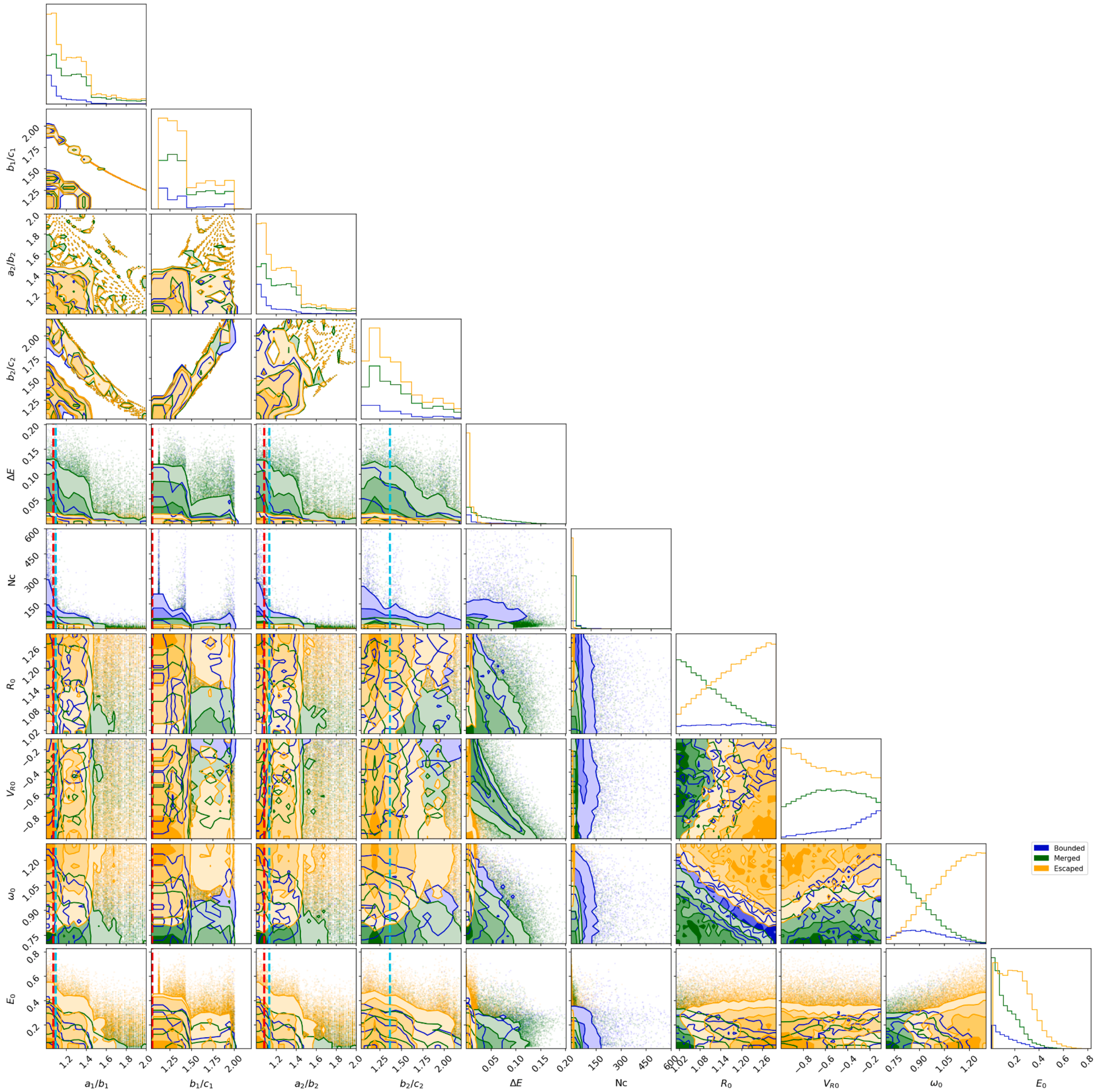

Fig. 9. Corner plot of randomized initial conditions. Blue represents bounded conditions, orange indicates escaped scenarios, and green represents merged outcomes for COR = 0.9.

We observed three distinct outcomes from the results: merged cases, bounded cases, and escaped cases. In the merged case, the bodies collide multiple times during their orbital evolution and lose enough energy, in a situation where their post-collision velocities are not sufficient to overcome gravitational attraction, eventually sticking together. In the bounded case, the components lose some energy but maintain an orbit in which, after a certain time, the number of collisions are small or inexistent. Finally, in the escaped case, an initially elliptic orbit becomes hyperbolic as a consequence of transferring rotational energy to orbital energy.

Now, assume that the principal axes of the ellipsoids are described by a_i, b_i and c_i, where $i = 1, 2$ represents the primary and secondary body, respectively. We will assume arbitrary values of f for each body (see Eq. (3)). In Fig. 4, we present a case of perfectly elastic conditions (COR = 1). It can be observed that the motion is bounded, and that the collision events cause changes in the direction of the linear velocity. The orbital frequency increases and decreases as the radial separation varies, in accordance with the conservation of angular momentum. As expected, the motion resembles a harmonic oscillator. On the other hand, in Fig. 5 we illustrate a case with energy dissipation to demonstrate the dissipation behavior and merging situation. The figure represents the time evolution of some dynamical variables and the reduced energy (E). The red vertical lines illustrate the collision events, and the initial conditions used for the simulations are detailed in Table A.1 of Appendix A. The early collisions caused higher energy dissipation

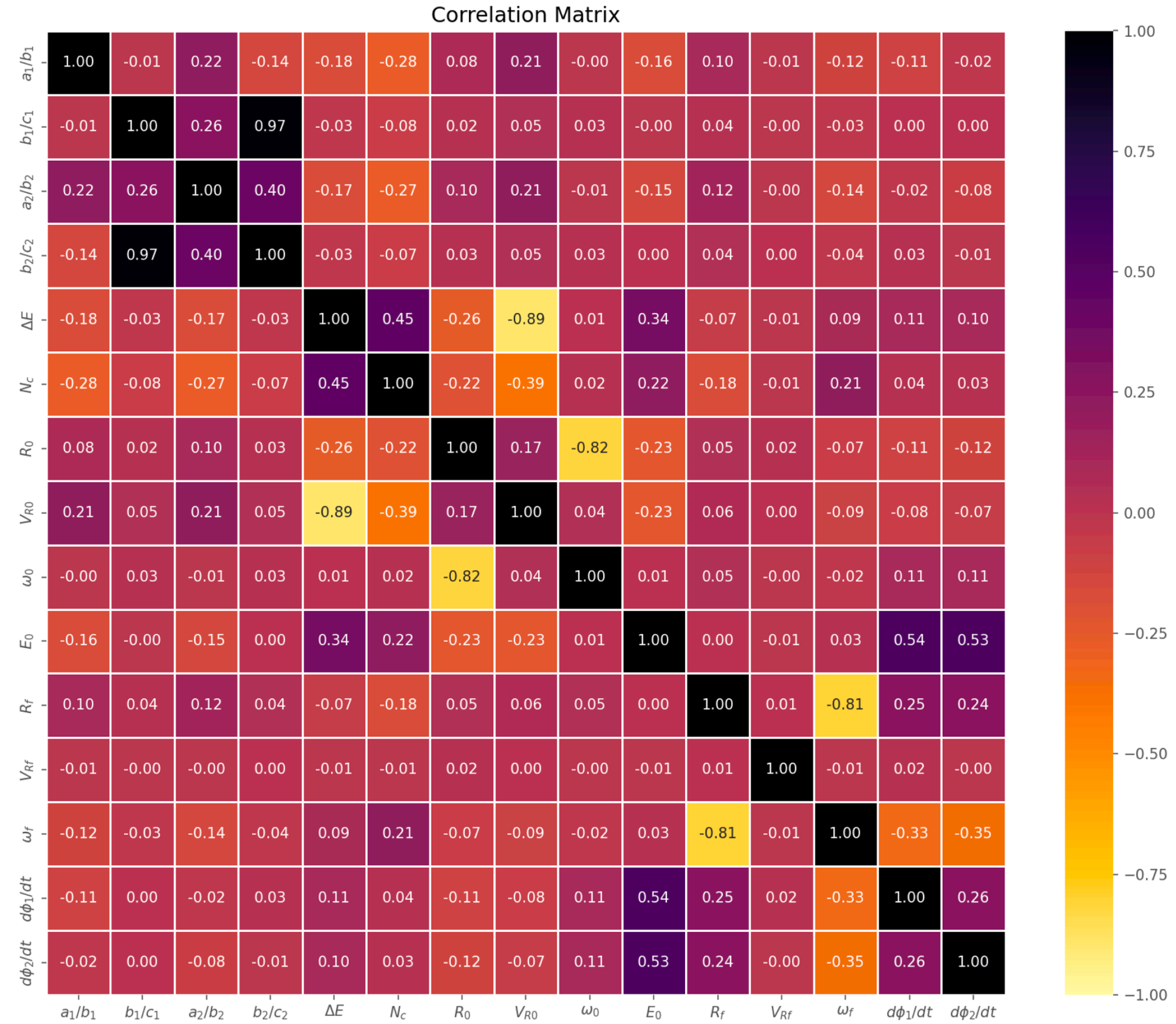

Fig. 10. Correlation matrix of the bounded cases for COR = 0.9.

because of the high relative velocity, and later collisions are less dissipative until a merged status is obtained. In this case, the system behaves like a non-continuous temporary damped harmonic oscillator.

In Figs. 6 and 7, we present a bounded example for different time scales. In contrast with the merged example, this case shows a situation where the system continues to rebound during the simulation time. Another example is illustrated in Fig. 8 for a bounded case, where collisions stop after approximately 850 revolutions and start again around 1400 revolutions.

6. Random sampling simulations

This paper focuses on understanding collisions between hard ellipsoids (no deformations), where the bodies are assumed to be initially in close proximity or just barely in contact with one another. To investigate the dynamical evolution of binary systems using the modeling approach described in Sections 2–4, we performed randomized simulations based on the initial state vector $\mathbf{Y}_0 = [R, \theta = 0, \phi_1, \phi_2, \dot{R}, \omega, \dot{\phi}_1, \dot{\phi}_2]$, with 882,000 simulation points.[3] The following considerations were made.

- The semi-axes of the ellipsoids are calculated using Eq. (3) for values of $a_0 = [0.5, 0.45]$, $b_0 = [0.45, 0.4, 0.35, 0.3]$ and $c_0 = [0.4, 0.35, 0.3, 0.25]$, always considering $a_0 > b_0 > c_0$ and f_i varying between 0 and 1;

[3] In this case $\omega = \dot{\theta}$.

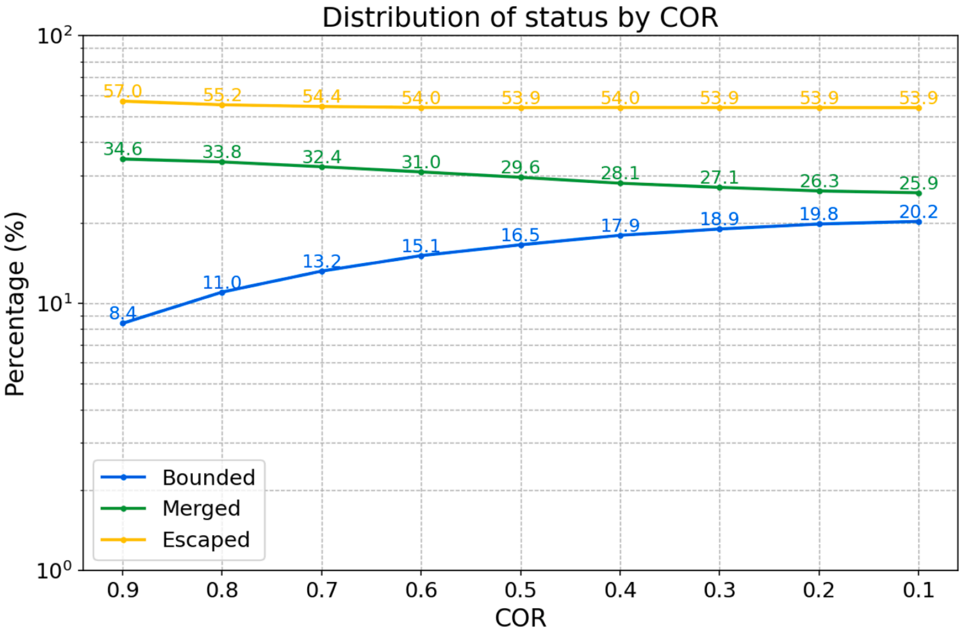

Fig. 11. Simulation outcomes percentage for each value of COR for bounded, merged, and escaped.

- The mass of each body is given by $M_i = \rho_i V_i$, where ρ_i is the body's density, with $\rho_1 = \rho_2 = \rho$, and $V_i = \frac{4}{3}\pi a_i b_i c_i$ is the volume of each ellipsoid;
- The constraint $M_1 + M_2 = 1.0$ implies that $a_1 b_1(f_1) c_1(f_1) + a_2 b_2(f_2) c_2(f_2) = \frac{3}{4\pi\rho}$, with $a_1 \geq a_2$;
- The mass-normalized inertia tensor of each body is calculated via Eq. (4).

For the initial separation, we assumed values between $1.01 < R < 1.3$, covering close contact to separations of one orbital semi-major axis. The initial rotational states were constrained to $-\pi/6 < \phi_i < \pi/6$ for $i = 1, 2$. The binary orbital angular velocity was assumed to be in the range $0.8 < \dot{\theta} < 1.2$, while the initial relative speed $-1.0 < \dot{R} < -0.1$, ensuring a collision trajectory. For the spin of each body, moderate values were selected within the range $-\pi/2 < \dot{\phi}_i < \pi/2$ radians per unity of time. This constrained the investigation to bodies with moderate rotation speeds, avoiding fission velocities. The equations of motion were evolved numerically until $\theta = 2000 \cdot 2\pi$, following the procedure described in Section 3. Initial conditions that did not complete 2000 revolutions were discarded. The minimum mass ratio was $\mu \approx 0.2$. For each initial condition we simulated the following values of $\mathrm{COR} = [0.1, 0.2, 0.3, 0.4, 0.5, 0.6, 0.7, 0.8, 0.9]$.

In Fig. 9 we present the corner plot for our simulations. A corner plot is a powerful visualization tool for statistical data analysis and Bayesian inference (see Foreman-Mackey [28]). Such diagram displays scatter plots for every pair of variables, with their distributions along the diagonal, providing a straightforward representation of relationships between variables. Here, we categorize the orbital outcomes of the 6770 different initial ellipsoids configurations assuming 25 random initial state vectors summarizing 135,400 simulations into three categories: bounded, merged, and escaped, represented by blue, green, and orange, respectively. The plot includes a_i/b_i and b_i/c_i for primary and secondary bodies ($i = 1, 2$), energy dissipation (ΔE), number of collisions (N_C), initial state variables R_0, $\dot{R}_0 = V_{R0}$, $\dot{\theta}_0 = \omega_0$, and initial energy E_0.

Fig. 9 reveals a strong relation between ω_0 and R_0, highlighting differences in data configurations and patterns across the three orbital outcomes, which was also observed for bounded binaries in [29]. A similar trend is observed for V_{R0}. Furthermore, ΔE shows that some configurations lose energy and escape. The plot also indicates that higher absolute initial velocities lead to greater energy dissipation during evolution. We also note that merged conditions are more concentrated at lower initial energies, while bounded systems continue to rebound reaching more than 200 collisions. Higher initial energies lead to increased escape rates (E_0) compared to other cases. The simulations suggest that a certain energy threshold is needed to sustain rebounding orbits. If enough energy is lost, the bodies merge, while escaped orbits that dissipate sufficient energy may transition to bounded or merged conditions. It is possible to observe an intersection region between the initial energy and the final conditions, indicating that for values between 0.015 and 0.030 of E_0, the system could escape, merge or stay bounded depending on the collision response.

It is interesting to observe the presence of bounded systems that continue rebounding during the analyzed time frame, experiencing between 600 and 10,000 collisions. Since energy dissipation is related to the relative velocity, if the system reaches a configuration where collisions occur at a small relative velocity, it will remain a bounded rebounding system for an extended period. Eventually, the cumulative time and number of collisions may result in sufficient energy loss, leading to a merged state.

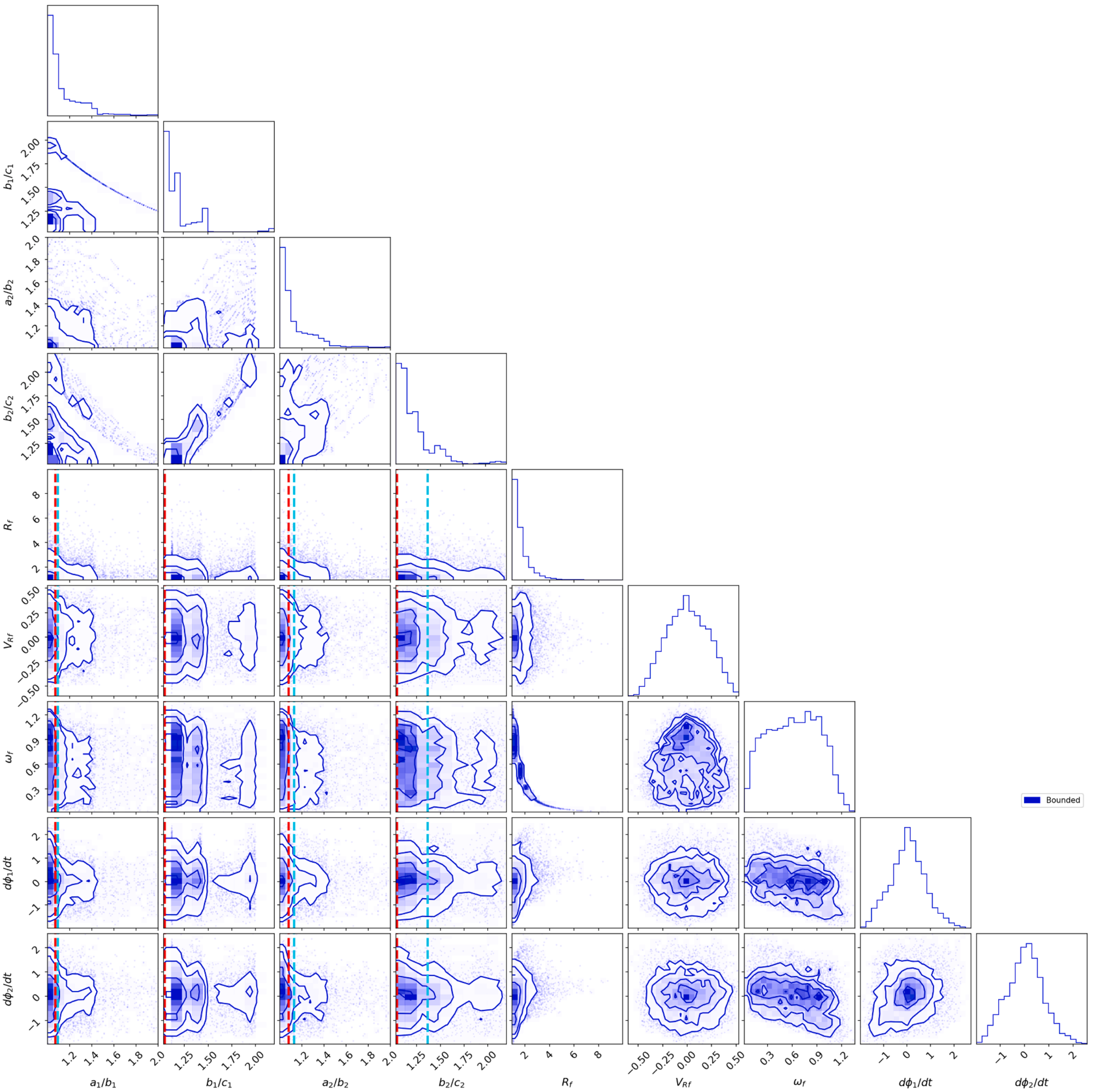

Fig. 12. Corner plot of randomized initial conditions for the bounded cases illustrating the ellipsoids parameters a/b and b/c with the instantaneous final states R_f, V_{Rf}, ω_f and the spins $d\phi_1/dt, d\phi_2/dt$ for COR = 0.9.

Let us now provide two physical examples. First, we indicate in Fig. 9 where the binary asteroid system (90) Antiope would fall within the randomized simulations by plotting red dashed lines corresponding to Antiope's deformations for the primary and secondary bodies. The primary asteroid has dimensions of $93.0 \times 87.0 \times 83.6$ km, with an average diameter of approximately 87.8 km, while the secondary asteroid measures $89.4 \times 82.8 \times 79.6$ km. The current separation between the two is 176 km. The second example is illustrated by the cyan dashed lines, representing (486958) Arrokoth, with dimensions of $22 \times 20 \times 7$ km for the primary lobe and $14 \times 14 \times 10$ km for the secondary lobe [30,31]. It is important to note that this assumption does not include the Arrokoth neck, which has dimensions ranging from 3.8 to 1.8 km [31]. Since the ratio of b/c for the primary lobe is too large, it is not shown in the plots. We will discuss these examples later in this section.

In Fig. 10, we illustrate a correlation matrix of the bounded cases which shows the linear relationship between different variables, in this case, the initial and final state variables and configurations of the randomized simulations. Variables with subscript 0 are the initial state, while f represents the final state. As expected we observe a strong negative correlation between the initial velocity and energy dissipation. A negative linear relationship was also observed between the initial separation and angular velocity ω_0, and a

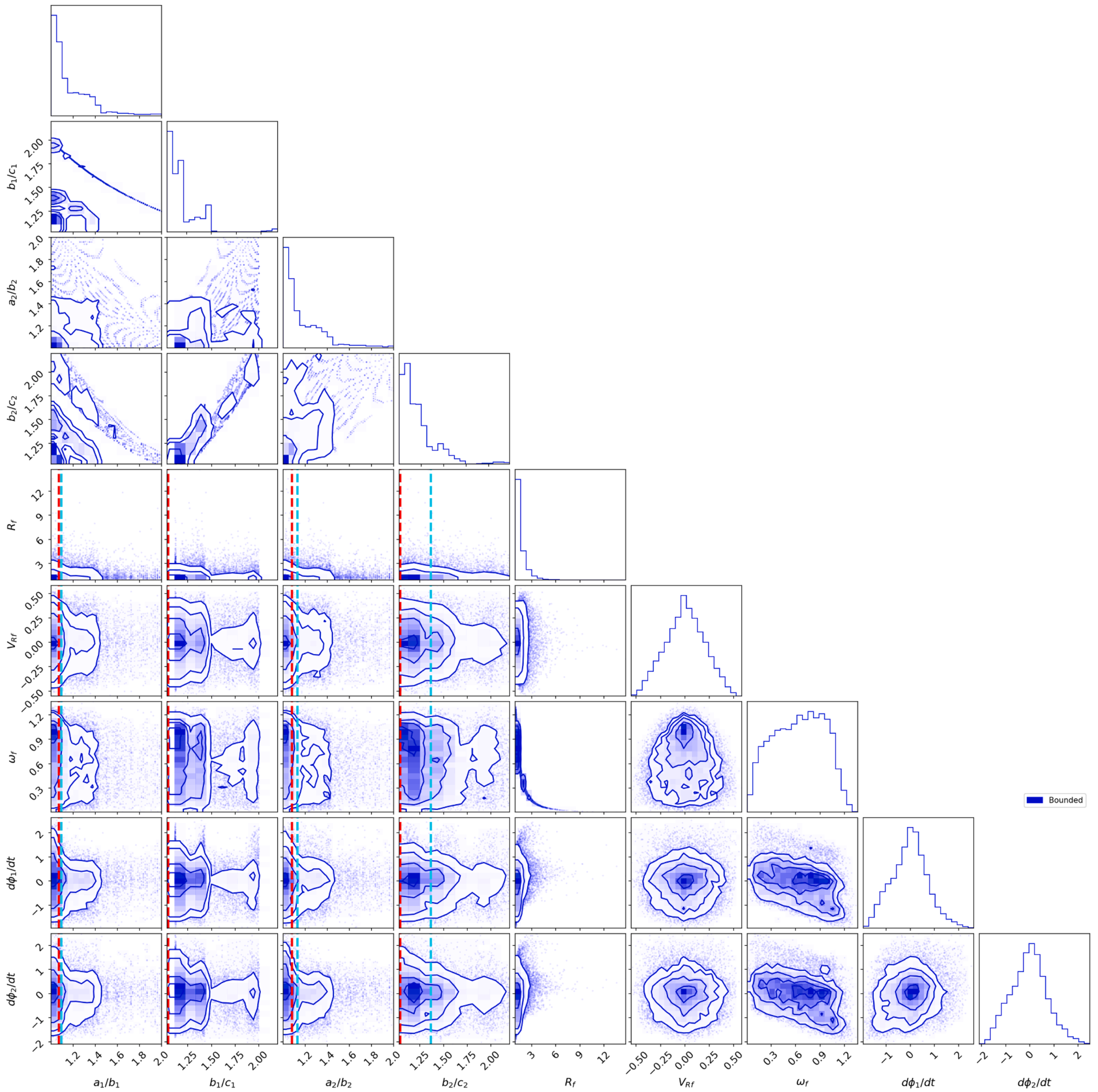

Fig. 13. Corner plot of randomized initial conditions for the bounded cases illustrating the ellipsoids parameters a/b and b/c with the instantaneous final states R_f, V_{Rf}, ω_f and the spins $d\phi_1/dt, d\phi_2/dt$ for COR = 0.5.

similar behavior was observed between the final separation and final angular velocity ω_f. The number of collisions N_c also shows a negative correlation of -0.21 with respect to the semi-axes relation a/b.

The percentage of randomized simulations that remain bounded, merged, or escaped is shown in Fig. 11 as a function of the coefficient of restitution. Overall, most of the outcomes correspond to escaped cases, with merged cases still accounting for an expressive amount of the results and only a small number of the simulations finishing in a bound state. Hence, it is easier for a colliding binary to separate than to merge, and it is even harder for both bodies to start orbiting each other. In addition, as we vary the COR from 0.9 to 0.1, the number of merged cases diminishes, while the number of bounded cases increases, meaning that collisions closer to a perfectly elastic behavior tend to form contact binaries.

In Figs. 12–14, we show isolated corner plots for COR 0.9, 0.5 and 0.1, including only cases which remain bounded after 2000 revolutions. In this plot, we are considering the instantaneous final states of the surviving initial conditions. It is possible to observe that after these many revolutions, the orbits tend to circularize, indicated by the final radial velocities concentrating around 0, with a higher distribution of points around $\omega_f = 1$. Similarly, the bodies' spins tend to approach 0, indicating spin-orbit coupling.

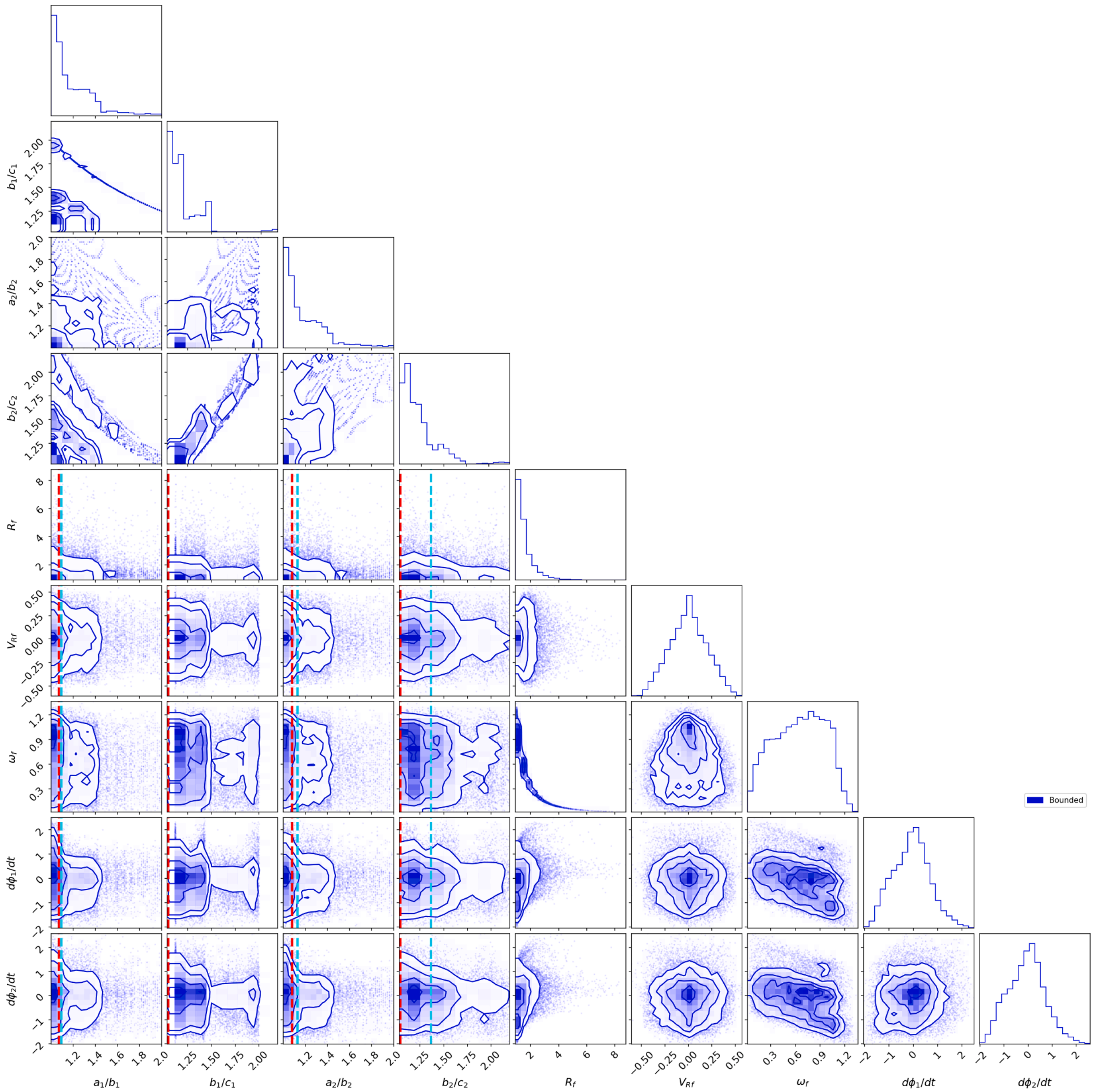

Fig. 14. Corner plot of randomized initial conditions for the bounded cases illustrating the ellipsoids parameters a/b and b/c with the instantaneous final states R_f, V_{Rf}, ω_f and the spins $d\phi_1/dt, d\phi_2/dt$ for COR = 0.1.

Furthermore, we observe a higher concentration of points in configurations close to spheroids with smaller ratios of a/b and b/c. As the coefficient of restitution is lowered, the dispersion of points around the equilibrium regions becomes more concentrated as seen, for instance, in the columns for ω_f, V_{Rf}, spins and separation. It is important to note that the difference observed between COR = 0.5 and COR = 0.1 is small compared to COR = 0.9.

In the results presented in Figs. 9, 12–14, we observe Antiope, represented by the red line, crossing regions with a highest chance for the system remaining bounded. However, this does not mean that the system cannot merge or escape; rather, the probability that any of these scenarios will happen depends on the initial conditions of the system, as indicated in Fig. 11. Observing the a_1/b_1, b_1/c_1 a_2/b_2, and b_2/c_2 ratios in Fig. 12, Antiope crosses regions with a high density of points related to the bounded scenario. For Arrokoth, a similar behavior is observed only for a_1/b_1 and a_2/b_2, while the others semi-axes ratios fall on regions with a much lower density of blue points. In this case, the probabilities of merging and remaining bounded are closer, with the main differences appearing in the semi-axis ratios, which also correspond to a lower chance of escaping.

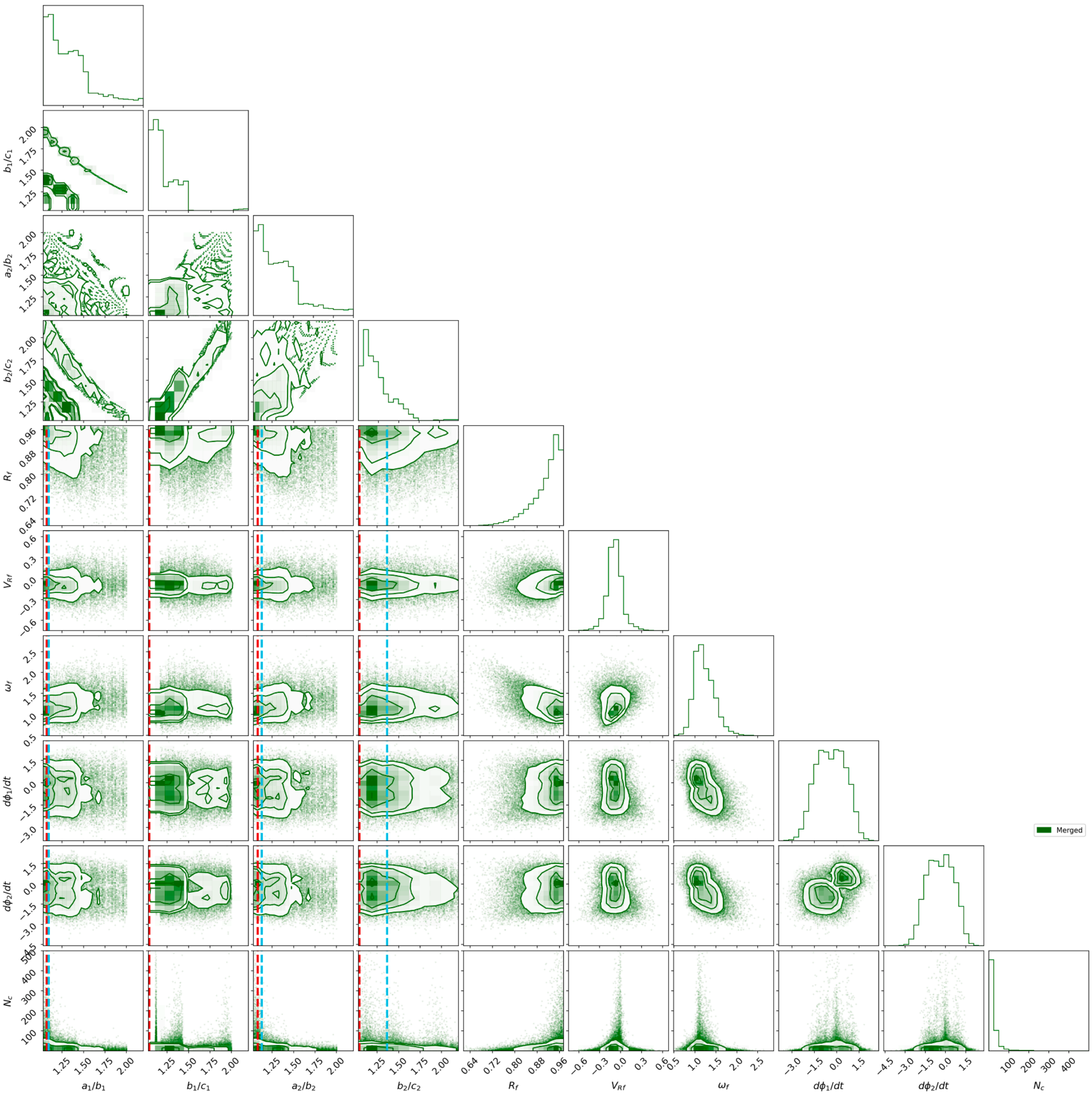

Fig. 15. Corner plot of randomized initial conditions for the merged cases illustrating the ellipsoids parameters a/b and b/c with the instantaneous final states R_f, V_{Rf}, ω_f, the spins $d\phi_1/dt, d\phi_2/dt$ and the number of collisions N_c for COR = 0.9.

Figs. 15–17 presents the corner plots focusing on the merge cases. From the bottom line, we can see that most merge events result from fewer than 100 collisions. However, there is a noticeable concentration of points near an expected equilibrium state, where the spin velocities are close to zero and $\omega_f \approx 1$. This behavior is not unusual, as in such cases the system may undergo a series of rebounds, gradually losing energy before finally reaching the merged state. However, this does not preclude the possibility of merging occurring at different velocities or radii. Although Antiope does not fully overlap the merging regions in all variables, particularly along the b/c axis, Arrokoth appears to closely intersect areas associated with the highest concentration of merged cases, especially in terms of spin rotation values. The supplementary material includes all corner plots for each of COR.

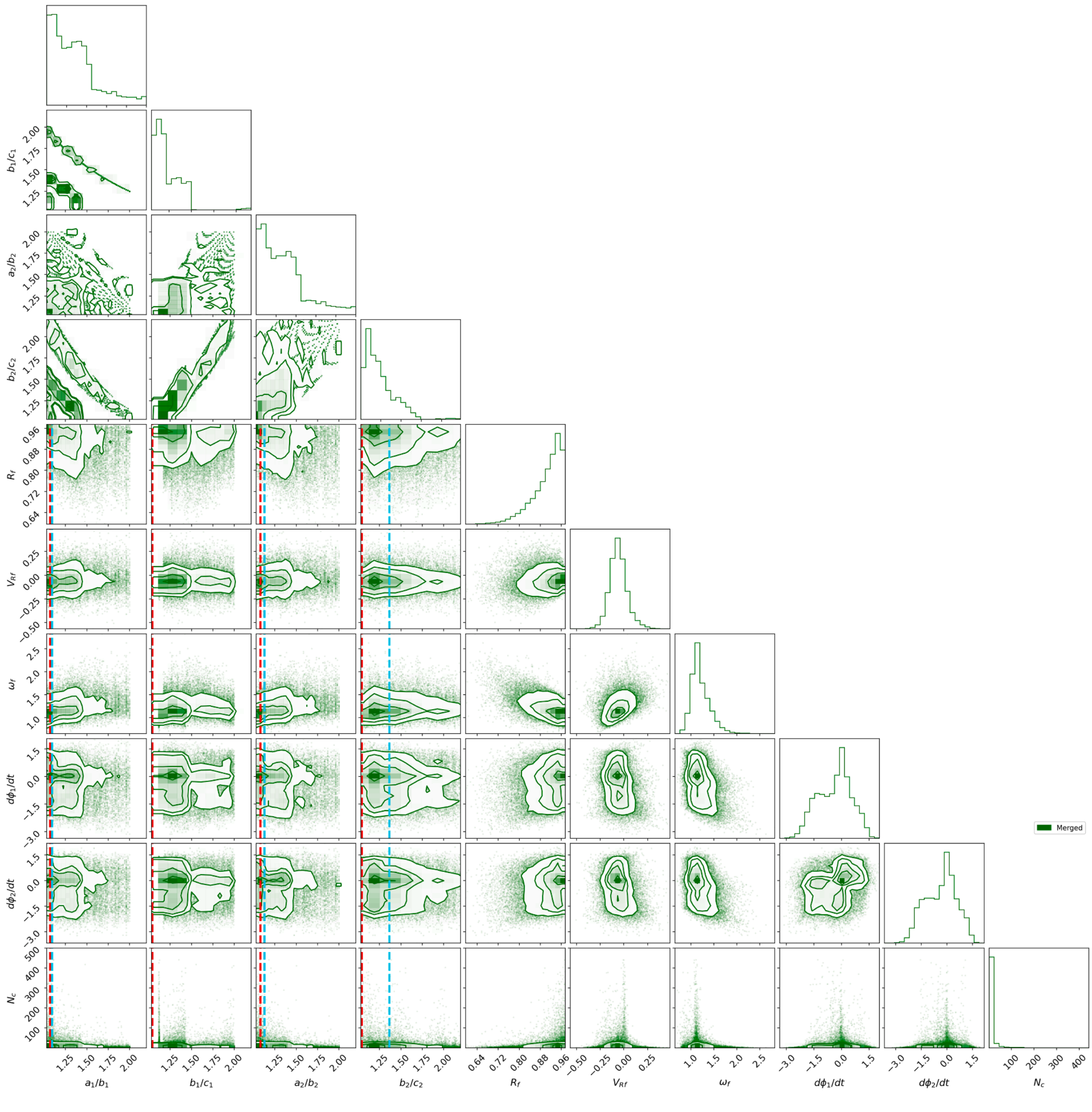

Fig. 16. Corner plot of randomized initial conditions for the merged cases illustrating the ellipsoids parameters a/b and b/c with the instantaneous final states R_f, V_{Rf}, ω_f, the spins $d\phi_1/dt, d\phi_2/dt$ and the number of collisions N_c for COR = 0.5.

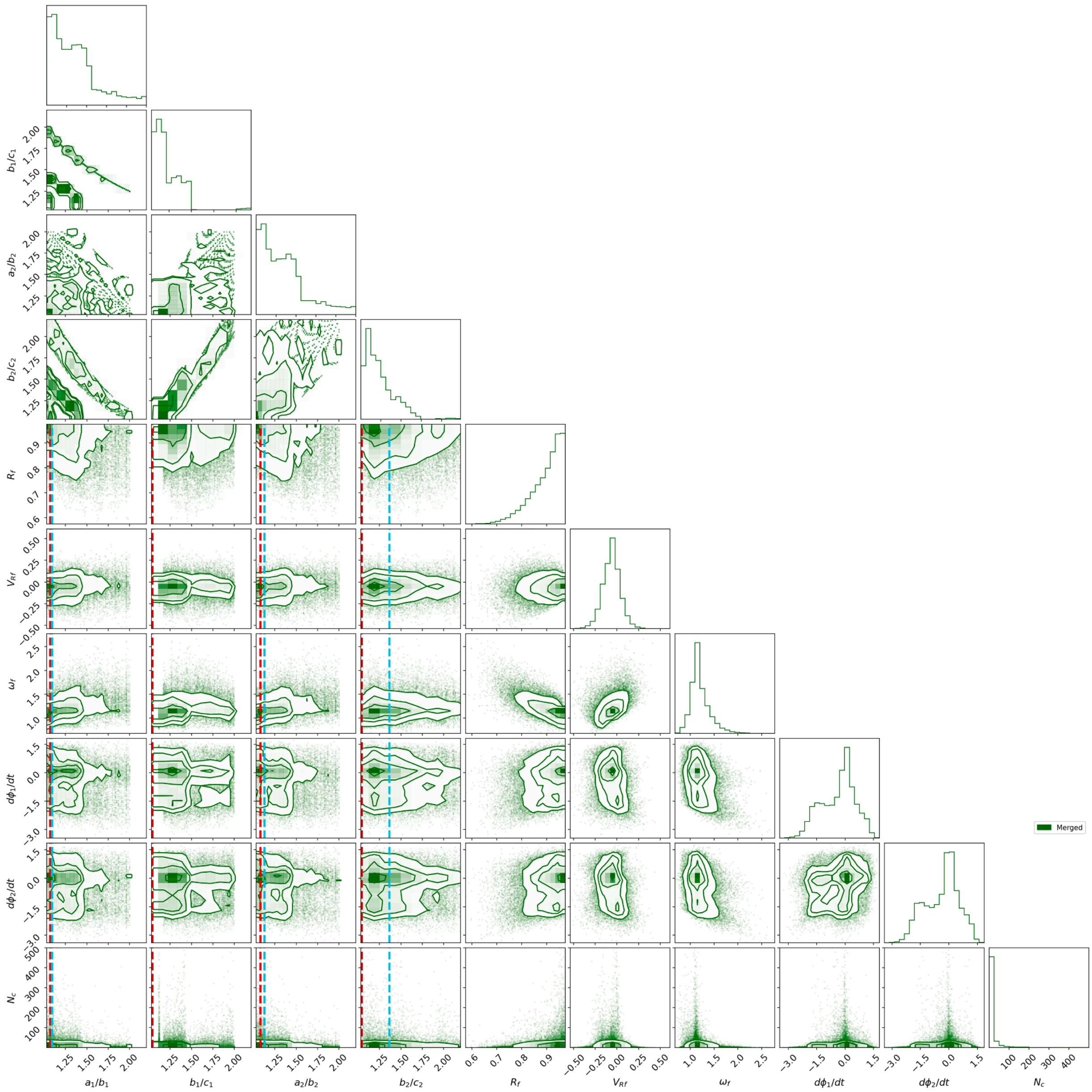

Fig. 17. Corner plot of randomized initial conditions for the merged cases illustrating the ellipsoids parameters a/b and b/c with the instantaneous final states R_f, V_{Rf}, ω_f, the spins $d\phi_1/dt, d\phi_2/dt$ and the number of collisions N_c for COR = 0.1.

7. Conclusion

In this paper, we explored the dynamical evolution of similar-sized binary systems within the framework of the F2BP model, focusing on the effects of energy dissipation over time due to low-velocity collisions between the bodies, assuming an impulse-response model for inelastic collisions. The randomized simulations allowed us to comprehensively investigate the interactions between the bodies as characterized by varying geometric eccentricities and densities. As a conclusion, we have observed that energy dissipation due to inelastic collisions plays a significant role in the formation of both contact and non-contact binary systems over short time scales.

Our results reveal a significant tendency for systems to escape, with a notable number of configurations becoming merged, and a small fraction rendering bounded systems. This underscores the dynamical complexity of such systems, where initial conditions play a crucial role in determining long-term outcomes. We found that merging typically occurs earlier than 2000 revolutions, whereas bounded systems often experience prolonged interactions, with some configurations undergoing more than 600 collisions. Furthermore, our analysis indicated that the nature of collisions significantly influences energy dissipation. Merged cases generally exhibited greater energy loss compared to bounded cases, suggesting that repeated low-velocity collisions may facilitate a gradual transition from a bounded to a merged state.

The present study has shown that our methodology could aid in the understanding of the dynamical evolution of small bodies such as bounded and contact/merging binaries. In the formation of (486958) Arrokoth, for example, low-velocity collisions were not previously considered. According to our results, simulations of Arrokoth's parameters showed a high likelihood of forming a binary contact system (see Fig. 9). As for the binary Antiope, our results have shown that there is a higher likelihood for the bodies to maintain a bounded orbit when comparing the corner plots of the bounded and merged cases.

It is important to note that the scheme adopted here operates under two specific assumptions: i) the energy dissipation model considers a constant coefficient of restitution which could be inadequate for large-scale collisions; ii) the mutual potential, derived as a 2nd order expansion in the bodies' inertia tensors, could be problematic for non-regular bodies with shapes far from spherical. Moreover, additional perturbations, such as solar radiation and tidal dissipation, undoubtedly influence the system's dynamical evolution over long time scales, potentially altering its final state. These effects will require more sophisticated models and longer computational times, and will be dealt with in future studies.[4]

CRediT authorship contribution statement

G. A. Caritá: Writing – review & editing, Writing – original draft, Visualization, Validation, Supervision, Methodology, Investigation, Funding acquisition, Formal analysis, Data curation, Conceptualization; **V. M. de Oliveira:** Writing – review & editing, Writing – original draft, Visualization, Validation, Software, Resources, Methodology, Investigation, Funding acquisition, Formal analysis, Data curation, Conceptualization; **S. Mottola:** Writing – review & editing, Supervision, Methodology, Data curation; **D. L. Silva:** Software, Methodology, Data curation; **S. Aljbaae:** Supervision, Software, Methodology, Formal analysis, Data curation; **H. Hussmann:** Writing – review & editing, Supervision, Methodology, Formal analysis, Data curation; **K. Willner:** Writing – review & editing, Methodology, Data curation; **A. F. B. A. Prado:** Supervision, Methodology, Formal analysis, Data curation.

Data availability

Data will be made available on request.

Declaration of competing interest

The authors declare the following financial interests/personal relationships which may be considered as potential competing interests: Gabriel Carita reports a relationship with State of Sao Paulo Research Foundation that includes: funding grants. V. M. de Oliveira reports a relationship with Fundação para a Ciência e a Tecnologia (FCT, Portugal) that includes: funding grants. Gabriel Carita reports a relationship with Coordination for the improvement of Higher Education Personnel that includes: funding grants. A. F. B. A. Prado reports a relationship with National Council for Scientific and Technological Devel386 opment (CNPq) that includes: funding grants. V. M. de Oliveira reports a relationship with State of Sao Paulo Research Foundation that includes:. If there are other authors, they declare that they have no known competing financial interests or personal relationships that could have appeared to influence the work reported in this paper.

[4] It is important to highlight that, while understanding that the mutual potential described in Scheeres [5,23] is based on a series expansion that suffers from divergence when objects overlap [12,32], our simulation stops when an object penetration occurs. Also, assuming a surface integral method [12] or even a polyhedral approach would highly increase the computational demand needed for the proposed random sampling investigation, causing it to be nonviable in this investigation due to the number of cases studied. As presented by Ho et al. [32], a newly fissioned contact binary system assuming the surface integral method and/or $\mathcal{O}(4)$ caused the computational time to increase by almost 20 times for a few hours of the system evolution.

Acknowledgements

This research was supported by resources supplied by the Center for Scientific Computing (NCC/GridUNESP) of the São Paulo State University (UNESP) and it was financed in part by Coordenação de Aperfeiçoamento de Pessoal de Nível Superior - Brasil (CAPES) - Finance Code 001 / PRInt 8887.829258/2023-00, National Council for Scientific and Technological Development (CNPq), under grant 309089/2021-2, 443116/2023-7, 403420/2024-5, São Paulo Research Foundation (FAPESP), under grants 2021/08274-9, 2021/11306-0, and 2022/12785-1, and Fundação para a Ciência e a Tecnologia (FCT, Portugal), under projects UIDP/04564/2020 and UIDB/04564/2020.

Appendix A. Initial conditions

In Table A.1 we detail the initial conditions used in this work alongside the corresponding figure number.

Table A.1
Initial conditions $\mathbf{Y}_0$ and masses M_1, M_2, for the Figures.

Figure	R	θ	ϕ_1	ϕ_2	$\dot{R}$	ω	$\dot{\phi}_1$	$\dot{\phi}_2$	M_1	M_2
4	1.02839	0.00	−0.265659	−0.442930	−0.720168	1.00821	1.07818	0.27680	0.54959	0.45040
5	1.021499	0.00	0.439523	0.16859	−0.97175	0.70915	−1.42781	0.77943	0.490263	0.50973
6, 7	1.13964	0.00	−0.3987413	−0.33144	−0.25045	0.83417	0.75258	−0.419962	0.49035	0.50964
8	1.23578	0.00	0.2287	−0.11729	−0.62341	0.82452	0.41418	−0.19609	0.5	0.49999

References

[1] Ćuk M. Formation and destruction of small binary asteroids. Astrophys J 2007;659(1):L57.
[2] Taylor PA, Margot J-L. Tidal end states of binary asteroid systems with a nonspherical component. Icarus 2014;229:418–22.
[3] Bottke W FJ, Melosh HJ. Binary asteroids and the formation of doublet craters. Icarus 1996;124(2):372–91.
[4] Pravec P, Vokrouhlický D, Polishook D, Scheeres DJ, Harris AW, Galad A, et al. Formation of asteroid pairs by rotational fission. Nature 2010;466(7310):1085–8.
[5] Scheeres DJ. Stability of binary asteroids. Icarus 2002;159(2):271–83.
[6] Scheeres DJ. Rotational fission of contact binary asteroids. Icarus 2007;189(2):370–85.
[7] Fahnestock EG, Scheeres DJ. Simulation of the full two rigid body problem using polyhedral mutual potential and potential derivatives approach. Celestial Mech Dyn Astron 2006;96:317–39.
[8] Hou X, Scheeres DJ, Xin X. Mutual potential between two rigid bodies with arbitrary shapes and mass distributions. Celestial Mech Dyn Astron 2017;127:369–95.
[9] Tricarico P. Figure–figure interaction between bodies having arbitrary shapes and mass distributions: a power series expansion approach. Celestial Mech Dyn Astron 2008;100:319–30.
[10] Conway JT. Vector potentials for the gravitational interaction of extended bodies and laminas with analytical solutions for two disks. Celestial Mech Dyn Astron 2016;125(2):161–94.
[11] Lu J, Shang H, Zhang X. A global binary asteroid system model with irregularly shaped components via iterated surface integral. Mon Not R Astron Soc 2025;536(1):592–602.
[12] Ho A. Modeling asteroid binary systems with the full two-body problem using surface integrals. Doctoral Dissertations at University of Agder 2023;.
[13] Trulsen J. On the rings of saturn. Astrophys Space Sci 1972;17:330–7.
[14] Bridges FG, Hatzes A, Lin D. Structure, stability and evolution of saturn's rings. Nature 1984;309(5966):333–5.
[15] Dilley JP. Energy loss in collisions of icy spheres: loss mechanism and size-mass dependence. Icarus 1993;105(1):225–34.
[16] Dilley J, Crawford D. Mass dependence of energy loss in collisions of icy spheres: an experimental study. J Geophys Res Planets 1996;101(E4):9267–70.
[17] Albers N, Spahn F. The influence of particle adhesion on the stability of agglomerates in Saturn's rings. Icarus 2006;181(1):292–301.
[18] Raman CV. The photographic study of impact at minimal velocities. Phys Rev 1918;12(6):442.
[19] Andrews JP. Experiments on impact. Proc Phys Soc 1931;43(1):8.
[20] Durda DD, Movshovitz N, Richardson DC, Asphaug E, Morgan A, Rawlings AR, et al. Experimental determination of the coefficient of restitution for meter-scale granite spheres. Icarus 2011;211(1):849–55.
[21] Descamps P, Marchis F, Michalowski T, Vachier F, Colas F, Berthier J, et al. Figure of the double asteroid 90 antiope from adaptive optics and lightcurve observations. Icarus 2007;187(2):482–99.
[22] McKinnon WB, Richardson DC, Marohnic JC, Keane JT, Grundy WM, Hamilton DP, et al. The solar nebula origin of (486958) arrokoth, a primordial contact binary in the kuiper belt. Science 2020;367(6481):eaay6620.
[23] Scheeres DJ. Stability of the planar full 2-body problem. Celestial Mech Dyn Astron 2009;104:103–28.
[24] Rackauckas C, Nie Q. DifferentialEquations.jl–a performant and feature-rich ecosystem for solving differential equations in Julia. J Open Res Software 2017;5(1), 15, https://doi.org/10.5334/jors.151.
[25] Gilitschenski I, Hanebeck UD. A robust computational test for overlap of two arbitrary-dimensional ellipsoids in fault-detection of kalman filters. In: 2012 15th international conference on information fusion. IEEE; 2012, p. 396–401.
[26] Nelder JA, Mead R. A simplex method for function minimization. Comput J 1965;7(4):308–13.
[27] Barraff D. An introduction to physically based modeling: rigid body simulation. Siggraph Course Notes 1997;1025.
[28] Foreman-Mackey D. corner.py: scatterplot matrices in python. J Open Source Software 2016;1(2):24. https://doi.org/10.21105/joss.00024
[29] Caritá GA, Hussmann H, Prado A, Callegari Jr N, Morais M, de Carvalho RE. Planar dynamics of non-spherical close tidally locked binaries and the restricted three body problem. Nonlinear Dyn 2025;113(13):16343–66.
[30] Stern SA, Weaver HA, Spencer JR, Olkin CB, Gladstone GR, Grundy WM, et al. Initial results from the new horizons exploration of 2014 MU69, a small kuiper belt object. Science 2019;364(6441):eaaw9771.
[31] Amarante A, Winter OC. Surface dynamics, equilibrium points and individual lobes of the kuiper belt object (486958) arrokoth. Mon Not R Astron Soc 2020;496(4):4154–73.
[32] Ho A, Wold M, Poursina M, Conway JT. The accuracy of mutual potential approximations in simulations of binary asteroids. Astron Astrophys 2023;671:A38.

Glossary

G	Gravitational constant.
M_1	Primary mass.
M_2	Secondary mass.
μ	Mass ratio $\frac{M_2}{M_1+M_2}$.
$\boldsymbol{I}_i$	Tensor of inertia of each body.
$\bar{\boldsymbol{I}}_i$	Mass-normalized tensor of inertia of each body.
R	Binary center of mass separation.
ϕ_1	Rotational state of the primary.
ϕ_2	Rotational state of the secondary.
$\dot{\phi}_1$	Spin of the primary in the z-axis.
$\dot{\phi}_2$	Spin of the secondary in the z-axis.
$\boldsymbol{\Omega}_1$	Angular velocity vector of the primary.
$\boldsymbol{\Omega}_2$	Angular velocity vector of the primary.
θ	Rotational state of the binary system.
$\dot{\theta}$	Binary system angular velocity.
a	Longest axis of the ellipsoid.
b	Intermediate-length axis of the ellipsoid.
c	Shortest axis of the ellipsoid.
f	Geometric eccentricity.
COR	Coefficient of Restitution.
m	Reduced mass $\frac{M_1 M_2}{M_1+M_2}$.
$K(\lambda)$	Function for ellipse overlapping.
$\mathbf{r}_1$	Distance from the center of mass of the primary ellipsoid to the collision point.
$\mathbf{r}_2$	Distance from the center of mass of the secondary ellipsoid to the collision point.
$\mathbf{v}_1$	Center of mass velocity of the primary ellipsoid.
$\mathbf{v}_2$	Center of mass velocity of the secondary ellipsoid.
$\mathbf{v}_{rel}$	Relative velocity at the point of contact.
ρ	Mass density.
$\mathbf{n}$	Normal direction of the collision plane.